

Experimental investigation of saturated pool boiling on a porous copper-graphene coating surface with microgrooves

Guochao Fei¹, Yanping Du^{2,*}

¹China-Uk Low Carbon College, Shanghai Jiao Tong University, Shanghai 201306, China

²School of Engineering, Lancaster University, Lancaster LA1 4YW, UK

³ Corresponding author's e-mail: y.du17@lancaster.ac.uk

Abstract. In this study, a microgroove porous copper-graphene composite coating was fabricated on a copper substrate utilizing a combination of salt template sintering and mechanical cutting. The pool boiling heat transfer performance of the modified surface was investigated with water as the working fluid at atmospheric pressure. The experimental results demonstrated that the integration of microgrooves with a porous copper-graphene coating substantially improved the pool boiling heat transfer performance. Among the tested configurations with 4, 6, 10, 18, and 24 microgrooves, the surface with 18 grooves exhibited the most superior performance, marked by an 82% reduction in the onset of nucleate boiling (ONB), a 189% increase in the critical heat flux (CHF), and a 140% enhancement in the heat transfer coefficient (HTC) compared to a smooth copper surface. Further analysis of bubble dynamics revealed that the microgroove porous copper-graphene coating promotes heat transfer by creating a gas-liquid separation structure at low heat flux and by extending the triple-phase contact line at higher heat flux, both of which contribute synergistically to the enhanced boiling performance.

1. Introduction

Pool boiling is an essential technology for industries such as integrated circuits, aerospace, and power generation, which demand efficient thermal management under high heat flux conditions. The dynamic properties of bubbles play a decisive role in the efficiency of pool boiling technology, including nucleation site density, bubble growth rate, and departure frequency, which collectively determine heat transfer performance[1]. Surface modification techniques for constructing surface structures have been widely studied to improve the bubble dynamics properties of pool boiling process[2].

Among these, porous structures have consistently been a research focus for scientists due to their potential to form numerous micro/nano-sized cavities that serve as nucleation sites, coupled with strong capillary forces that enhance liquid wicking. Research has shown that porous copper surfaces often outperform their nickel counterparts, primarily due to copper's superior thermal conductivity, which accelerates bubble nucleation and enhances HTC[3]. Lv et al.[4] demonstrated that diamond particles could form robust metallurgical bonds with copper, thereby reducing thermal contact resistance and improving both nucleation rates and overall boiling performance. Similarly, Butler et al.[5] observed significant enhancements in heat transfer performance after adding a porous layer just 25 μm thick to a smooth copper surface. Additionally, Ma et al.[6] developed gradient pore structures by stacking and sintering materials of different particle sizes, which optimized bubble detachment and facilitated liquid backflow.

However, challenges remain. Zhang et al.[7] highlighted potential drawbacks associated with multiscale porous structures, noting that small pore channels may retain bubbles during the later stages of boiling, impeding effective gas-liquid separation and delaying surface rewetting. Furthermore, while increasing the thickness and decreasing the pore size of porous structures can increase nucleation site density and capillary forces, this can also lead to higher flow resistance between bubbles and liquid, thereby obstructing gas-liquid backflow[8] and increasing thermal resistance[9], ultimately reducing CHF and HTC.

In the quest to address the drawbacks of porous structures, this study introduces a novel microgroove porous copper-graphene composite coating applied to a copper substrate. Comparative experiments were conducted to assess the performance of this microgroove surface relative to non-grooved porous and smooth copper surfaces. High-speed photography technology is employed to capture and analyze the morphology of bubbles and fluids, to elucidate the role of the microgroove structure and graphene in influencing bubble dynamics and improving heat transfer efficiency.

2. Experiment preparation

2.1. Experiment materials

Copper powder was purchased from Beijing InnoChem Science & Technology Co., Ltd, with an average particle diameter of 20 μm . Graphene, was obtained from Saen Chemical Technology Co., Ltd, with an average single sheet diameter of 0.5 to 5 μm and an average thickness of less than 8 nm.

2.2. Surface synthesis

The graphene/copper powder coating composite was prepared using the ball milling method. A certain amount of graphene was mixed with copper particles by oscillation and then added to a ball mill, where it was milled at a speed of 700 rpm for 1 hour. After thorough milling, sodium bicarbonate particles and sintering oil were added to the milled mixture, ensuring that the total weight ratio of sodium bicarbonate, sintering oil, and powder was 1/3:1/2:1. The mixture was stirred evenly to obtain the coating composite.

Copper sheets, measuring 20 mm \times 20 mm \times 3 mm, were subjected to mechanical processing to create microgrooves. The bottom width of the rectangular microgroove is 400 μm , and the wall height of the microgroove is 300 μm . The number of microgrooves on the copper sheet surfaces was 4, 6, 10, 18, and 24, which is indicated in Figure 1.

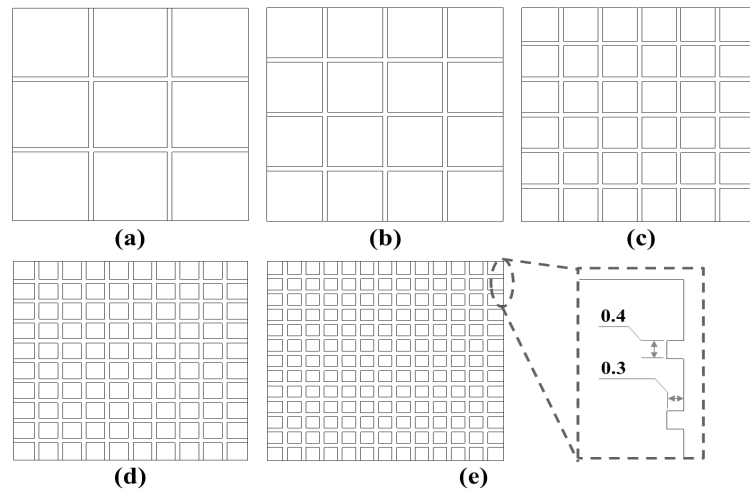


Figure 1. Microgroove copper surface structure: (a) 4 grooves, (b) 6 grooves, (c) 10 grooves, (d) 18 grooves, (e) 24 grooves.

The copper sheets were polished sequentially using 600-grit, 1000-grit, and 2000-grit sandpaper. They were then cleaned with deionized water and anhydrous ethanol. Following this, the coating mixture was applied to the samples using a screen-printing technique. The coated samples are subsequently sintered in a nitrogen atmosphere. The initial temperature is set to 450°C and maintained for 30 minutes. Then, the reaction temperature is increased to 800°C and held for 1 hour. After sintering, the samples are placed in a room temperature water bath for 2 hours, followed by drying at 60°C for 20 minutes.

Table 1. Sample names.

name	sample
smooth	Smooth copper surface
0-microgroove	Copper surface with a sintered porous copper-graphene coating, without microgrooves
4-microgroove	Copper surface with 4 microgrooves and a sintered porous copper-graphene coating
6-microgroove	Copper surface with 6 microgrooves and a sintered porous copper-graphene coating
10-microgroove	Copper surface with 10 microgrooves and a sintered porous copper-graphene coating
18-microgroove	Copper surface with 18 microgrooves and a sintered porous copper-graphene coating
24-microgroove	Copper surface with 24 microgrooves and a sintered porous copper-graphene coating

3. Experimental equipment and statistics processing

3.1. Pool boiling platform

The pool boiling experiment was conducted under atmospheric pressure in a saturated water boiling environment, as shown in Figure 2. By altering the operating voltage of the heating rods through a transformer, the temperature of the heating block is controlled to study the boiling performance of the surface under different heat flux conditions.

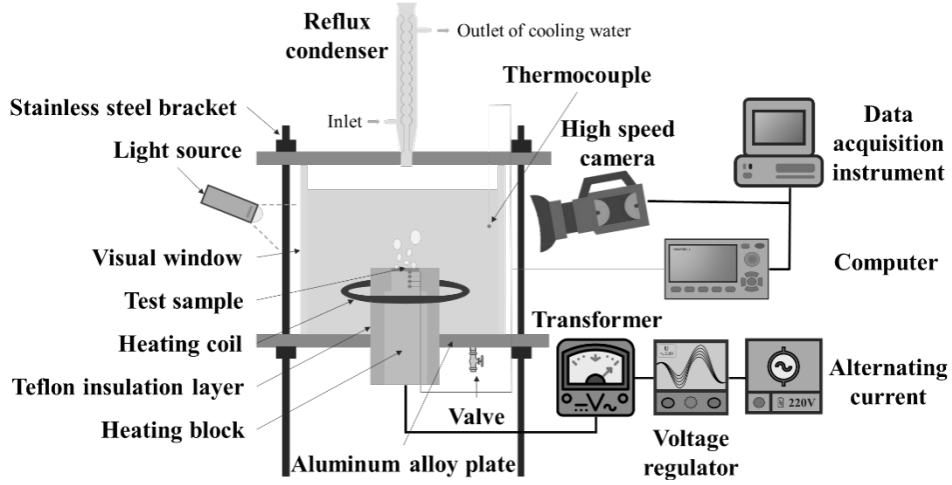


Figure 2. Pool boiling experimental system.

3.2. Data reducing

When the temperature stabilizes, the heat flux of heating block equals the instantaneous heat flux of the sample and remains constant. In this state of pool boiling, the following equation applies:

$$q = -k_{Cu} \cdot (T_0 + T_1 - T_2 - T_3)/4\Delta d \quad (1)$$

$T_0 \sim T_3$ are the temperatures measured by a set of thermocouples from top to bottom on the heated copper column, spaced evenly apart. Δd is the width of the adjacent temperature measurement points on the heated copper block, which is 7 mm.

According to the steady-state heat transfer model, the wall temperature and pool boiling heat transfer coefficient are derived from the following formulas:

$$T_w = T_0 + (T_1 - T_0) \cdot d_s/\Delta d \quad (2)$$

$$h = q \div (T_w - T_l) \quad (3)$$

T_w is the wall temperature, representing the temperature at the top of the surface. d_s is the sample thickness. h is the boiling heat transfer coefficient. T_l is the coolant temperature. The degree of wall superheat in the boiling experiment is calculated by:

$$\Delta T = T_w - T_l \quad (4)$$

ΔT is the wall superheat of the sample. The bubble detachment diameter is analyzed using the number of pixels in high-speed camera screenshots via Image J software. The bubble detachment frequency is calculated by analyzing the number of frames captured in the film.

3.3. Uncertainty analysis

The calculation of boiling heat transfer performance parameters utilized thermocouple temperature readings, the distance between thermocouples, and the thermal conductivity. In this study, the uncertainty of these parameters was determined using the error analysis theory proposed by McClintock and Kline[10]. The calculated uncertainties were found to be 7% for heat flux, 13% for wall temperature, and 8% for the heat transfer coefficient.

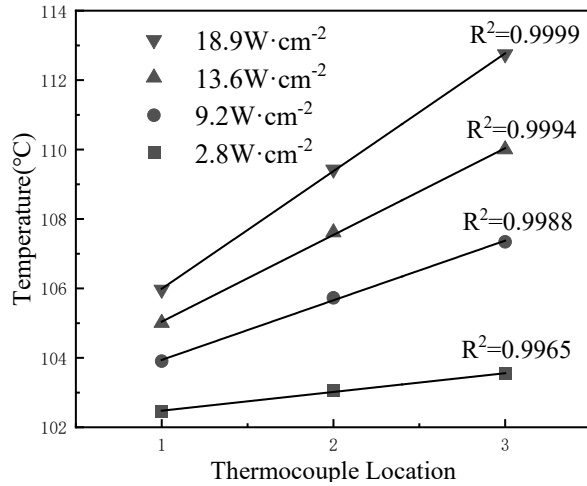


Figure 3. One-dimensional heat conduction verification diagram.

During the process where the heat flux increased from $2.8 W \cdot cm^{-2}$ to $18.9 W \cdot cm^{-2}$, the measured temperatures remained close to a linear trend, which is illustrated in Figure 3. As the temperature rose, the deviations decreased, approaching a state of one-dimensional heat conduction.

4. Results and Discussion

4.1. Microscopic characterization

Scanning electron microscope (SEM) images and Energy-dispersive X-ray spectroscopy (EDS) graphs of the ball-milled copper-graphene composite particles (Figure 4) reveal that graphene is effectively dispersed within the nano-scale crevices. This dispersion forms a strong composite structure that notably increases the thermal conductivity of the copper.

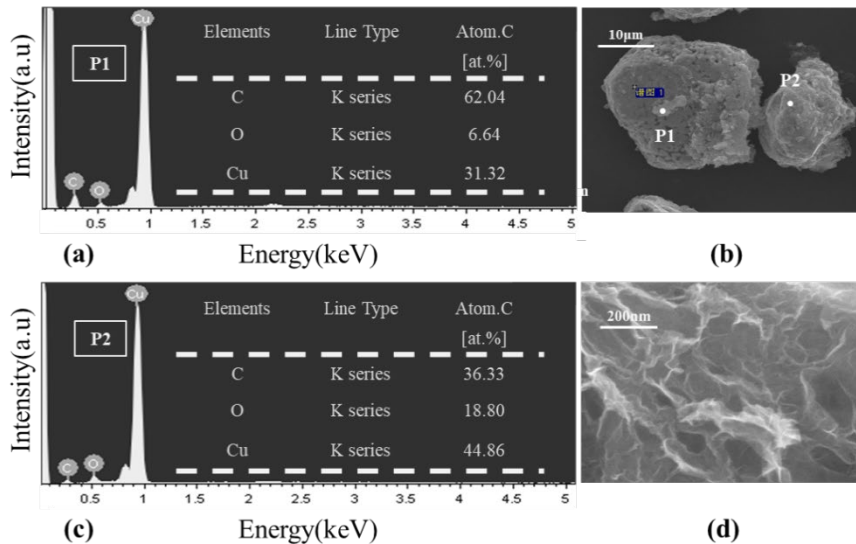


Figure 4. Microstructure characterization: (a) EDS of position P1, (b) EDS mapping of porous copper-graphene composite particles, (c) EDS of position P2, (d) SEM image of graphene.

The inner walls and bottoms of the grooves in the microgroove porous copper-graphene coating are uniformly covered with a porous copper-graphene particle layer. Within this coating,

numerous micro- and nano-sized pores interconnect to form microchannels on the copper surface, which is shown in Figure 5 and Figure 6.

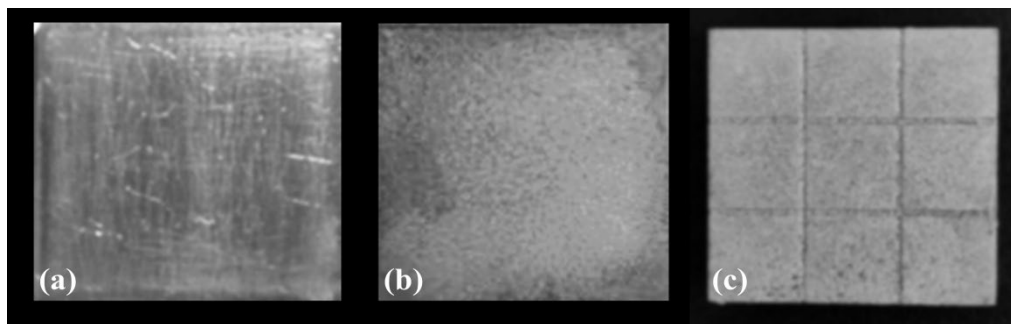


Figure 5. Sample surface: (a) smooth copper surface, (b) porous copper-graphene coating surface, (c) porous copper-graphene coating surface with four microgrooves.

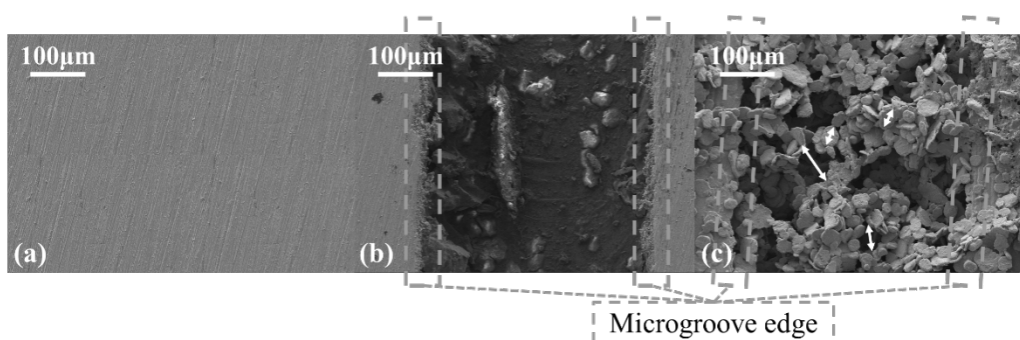


Figure 6. SEM images: (a) smooth copper surface, (b) copper surface with the microgrooves, (c) sintered copper-graphene coating surface with the microgrooves.

After sintering, both the microgroove copper-graphene coating surface and the copper-graphene coating surface exhibit superhydrophilicity, which is responsible for the capillary forces observed within the porous coating. As to the contact angle, upon peeling off the coating, copper-graphene coating surface with microgrooves is measured at 52° , as depicted in Figure 7-d, while copper-graphene coating surface is 57° . The minimal difference in contact angles between the two surfaces suggests that the superhydrophilicity is primarily attributed to the coating itself and the effect of microgrooves on the wettability of porous copper-graphene composite coatings is minimal.

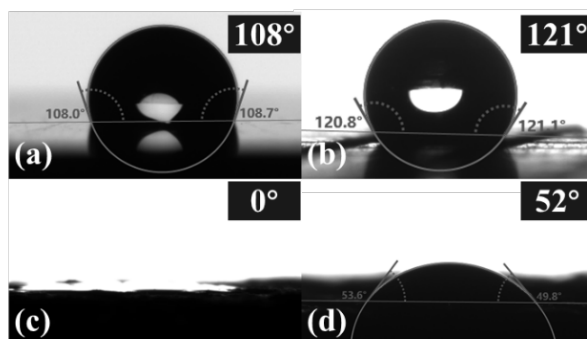


Figure 7. Contact angles: (a) smooth copper surface, (b) microgroove copper surface, (c) surface of the porous copper-graphene coating on the microgrooves, (d) surface of the microgroove porous copper-graphene coating after the sintered coating was peeled off.

4.2. Boiling Heat Transfer Performance

The pool boiling performance of the porous copper-graphene coating surface significantly exceed those of the smooth, whether in terms of ONB or CHF. This enhancement is attributed to the abundant active nucleation sites created by the micro/nano-scale pores within the porous structure and the improved liquid superheating enabled by the ultra-high thermal conductivity of graphene, as illustrated in Figure 8. When the density of microgrooves on the surface increases, the ONB of the porous copper-graphene coating surface decreases progressively, reaching a near-minimum value of 1.1 K when the number of grooves exceeds 10. The proximity of the microgroove bottom to the heat source, along with hindered convection, facilitates heat accumulation, thereby accelerating liquid superheating and promoting bubble nucleation and growth. Simultaneously, as the number of grooves increases, the CHF initially rises and then declines, peaking at $94.3 \text{ W}\cdot\text{cm}^{-2}$ when the sample is the 18-microgroove. This inflection point is associated with the suppression of gas-liquid separation effects. Compared to the smooth, the ONB is reduced by 82%, while the CHF is increased by 189%; relative to the 0-microgroove, the ONB is reduced by 70%, and the CHF is increased by 102%.

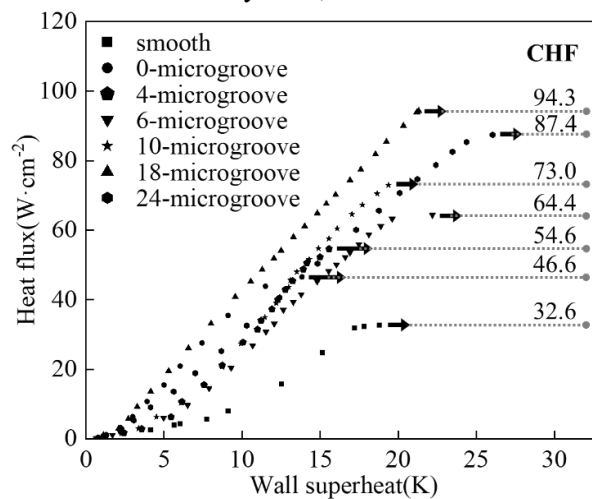


Figure 8. Heat flux variation curves of the porous copper-graphene coating surfaces with different numbers of microgrooves.

Table 2. The ONB of samples

name	ONB	name	ONB
smooth	6.0	10-microgroove	1.2
0-microgroove	3.7	18-microgroove	1.1
4-microgroove	1.2	24-microgroove	1.1
6-microgroove	1.7		

The HTC of the microgroove porous copper-graphene coating surface consistently surpasses that of the smooth, as depicted in Figure 9. The HTC for the 18-microgroove configuration reaches a peak value of $44.4 \text{ kW}\cdot\text{m}^{-2}\cdot\text{K}^{-1}$, representing a 140% improvement over the smooth and a 14% enhancement compared to the 0-microgroove. This indicates that a certain density of microgrooves can significantly improve the pool boiling heat transfer performance of the porous copper-graphene coating surface. At relatively low heat flux, the microgroove porous

copper-graphene composite coating achieves maximum HTC and maintains a stable, gradually increasing trend at higher heat flux densities. This behavior is attributed to the porous coating on the microgroove surface, which efficiently replenishes water to the nucleation sites via capillary action, effectively mitigating the expansion of dry areas.

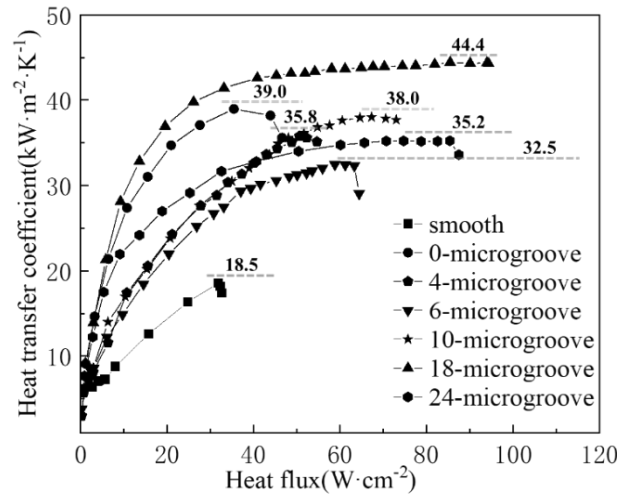


Figure 9. The different curves of heat transfer coefficient on the microgroove porous copper-graphene composite coated surfaces with different numbers of microgrooves.

4.3. Bubble Dynamics

The bubble diameters on the surface of the porous coating are smaller than those on the smooth, at low heat flux, as shown in Figure 10a. This phenomenon is attributed to the restrictive volume of pores within the coating, which limits bubble expansion, and the reduced contact angle caused by the copper-graphene particle coating. Additionally, the capillary forces within the microchannels of the porous coating enhance the liquid flow rate, creating a gas-liquid separation structure along the microgroove surface and the bubble rise channel, thereby reducing bubble growth and departure cycles, as illustrated in Figure 10b. As the heat flux increases, numerous nucleation sites within the porous coating are activated. Rapidly growing bubbles coalesce along the groove walls, forming larger bubbles that accelerate necking and detachment. After the addition of microgrooves, both the diameter and frequency of the bubbles have increased on the porous copper-graphene coating surface.

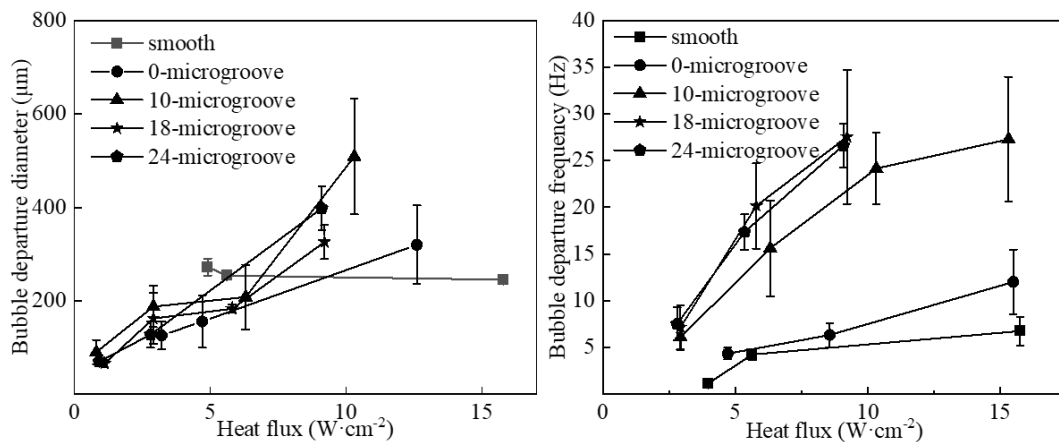


Figure 10. Curves of bubble departure diameter and frequency on porous copper-graphene composite coating surface with different number of grooves.

The porous copper-graphene coating, at low heat flux, owing to its high thermal conductivity, increased density of micro/nano-pores, and greater roughness, activates more bubble nucleation sites, resulting in a significantly higher bubble count compared to the smooth. The microgrooves further amplify this trend by expanding the nucleation area, leading to the generation of more bubbles, as shown in Figure 11. However, with denser microgrooves, bubble coalescence becomes more likely. As the heat flux increases, the gas-liquid separation effect weakens, forming a vapor film, thereby reducing boiling heat transfer efficiency.

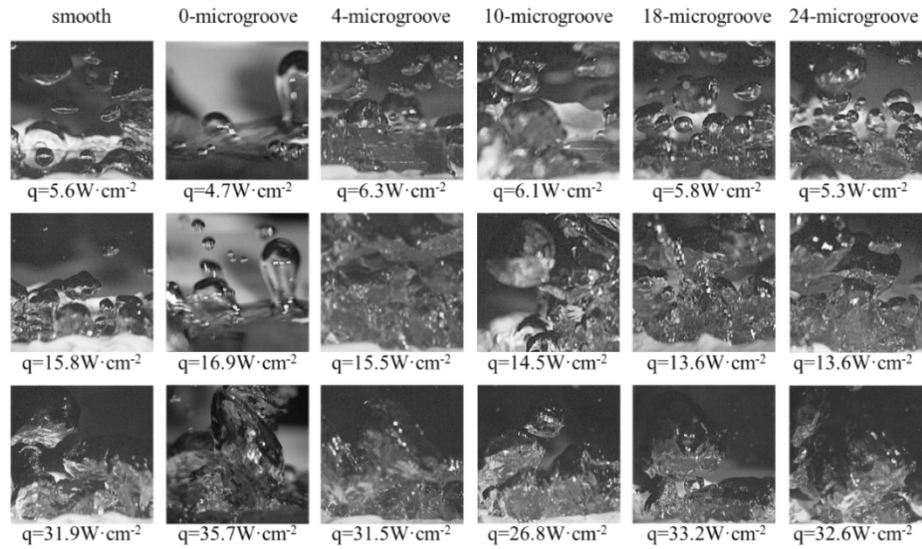


Figure 11. Bubble images on the surface of microgroove porous copper-graphene coatings with different groove densities under varying heat flux densities.

In summary, under different heat flux densities, the combined effects of various structural factors result in distinct bubble growth behaviors on the microgroove porous copper-graphene coating surface, which is indicated in Figure 12. At low heat flux, graphene effectively reduces the structural thermal resistance of the porous coating, accelerating liquid superheating at the bottom of the microgrooves and activating nucleation sites at a lower superheat degree. At the same heat flux, a larger number of bubbles nucleate, grow, and coalesce at the bottom of the microchannels, eventually detaching along the channels. Meanwhile, the porous coating continuously wicks the working fluid into distant areas along the inner walls of the microgrooves through capillary action, creating separated liquid and gas flow channels. This reduces bubble micro-convection interference and, compared to a planar surface, forms a channel pressure that promotes bubble detachment, thereby enhancing pool boiling performance, which is illustrated in Figure 12a. Under high heat flux, the active nucleation sites on the top of porous copper-graphene coating surface with microgrooves, which were not nucleated at low heat flux, are activated, with rapidly growing vapor cores merging with bubbles generated by the microgrooves. These large bubbles span multiple microgrooves, disrupting gas-liquid separation and slowing down the return flow of the working fluid. However, the movement of large bubbles increases the meniscus at the bottom of the microgrooves, and the enlarged three-phase contact line intensifies liquid film evaporation at the bubble base, further enhancing pool boiling performance, which is illustrated in Figure 12b.

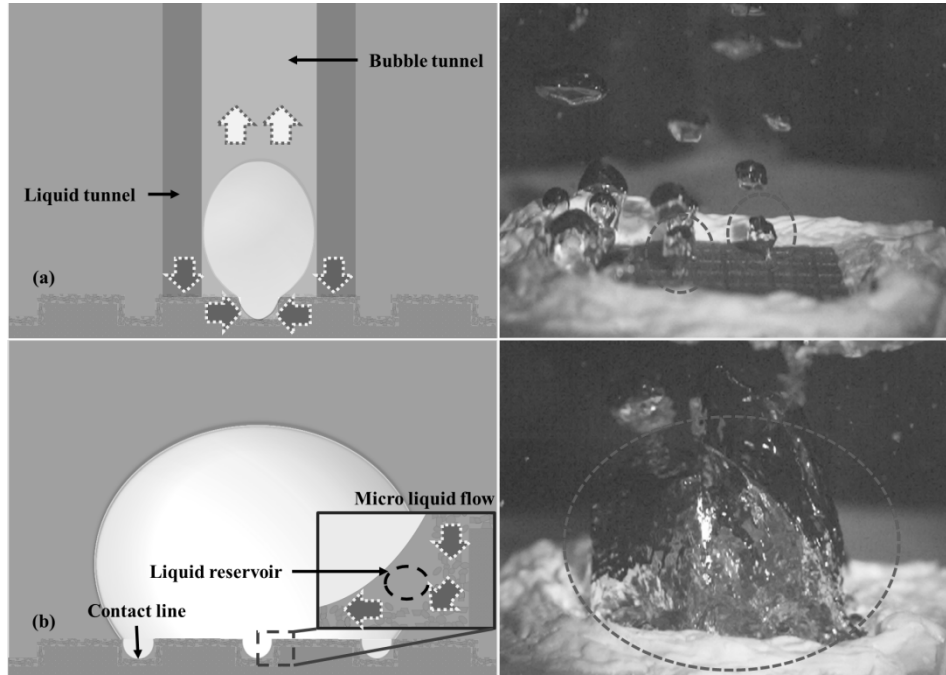


Figure 12. Schematic diagrams of bubble growth on the surface of microgroove porous copper-graphene coatings: (a) low heat flux, (b) high heat flux.

5. Conclusion

This study successfully combines the superior bubble nucleation capability of porous copper-graphene coatings with the geometric benefits of microgrooves, achieved through high-temperature sintering and mechanical cutting, to analyze the impact of varying microgroove numbers on pool boiling performance. The findings elucidate the mechanisms through which microgrooves enhance the boiling performance of porous copper-graphene coating surfaces, supported by detailed analyses of surface morphology, wettability, and bubble dynamics.

Firstly, the porous copper-graphene coating, characterized by its reduced structural thermal resistance and a high density of micro/nano-pores, significantly improves nucleation capabilities, leading to enhanced pool boiling performance compared to the smooth. This improvement underscores the critical role of the porous structure in facilitating efficient heat transfer through the generation of numerous active nucleation sites.

Secondly, the incorporation of microgrooves further reduces ONB on the porous copper-graphene composite surface. This reduction is attributed to the proximity of the microgroove bottoms to the heat source, which promotes accelerated liquid superheating from multiple sides. Additionally, the microgrooves substantially increase the maximum HTC and CHF. Notably, the 18-microgroove achieved a 14% improvement in HTC and a 102% enhancement in CHF compared to the configuration without microgrooves. When compared to the smooth, these enhancements are even more pronounced, with ONB reduced by 82%, and CHF and HTC increased by 189% and 140%, respectively.

Thirdly, at low heat flux, the microgrooves effectively separate gas-liquid flow channels, creating a channel pressure that facilitates bubble rise and increases bubble departure frequency, thereby enhancing pool boiling heat transfer. However, at high heat flux, the denser microgrooves tend to cause smaller bubbles to coalesce into larger bubbles that can cover the

surface, thereby weakening the gas-liquid separation effect. Despite this, the presence of microgrooves at the base of large bubbles increases the three-phase contact line, which promotes vigorous evaporation of the meniscus liquid, ultimately enhancing both CHF and HTC.

Acknowledgments

This work was financially supported by the National Key Research and Development Program (No.2022YFE0198800), and the National Natural Science Foundation of China (No. 52076139).

References

- [1] Chu H, Yu X, Jiang H, Wang D and Xu N (2023) Progress in enhanced pool boiling heat transfer on macro- and micro-structured surfaces. *International Journal of Heat and Mass Transfer*, 200:123530.
- [2] Tang H, Guo B, Tang Y, Wu X, Peng R and Sun Y (2022) Fabrication and boiling heat transfer characterization of multi-scale microgroove surfaces. *Science China Technological Sciences*, 65:3010-3019.
- [3] An Y, Huang C and Wang X (2021) Effects of thermal conductivity and wettability of porous materials on the boiling heat transfer. *International Journal of Thermal Sciences*, 170:107110.
- [4] Lv Z, An Y and Huang C (2023) Enhanced pool boiling heat transfer by adding metalized diamond in copper porous materials. *Applied Thermal Engineering*, 226:120288.
- [5] Butler AP, James GB, Maddock BJ and Norris WT (1970) Improved pool boiling heat transfer to helium from treated surfaces and its application to superconducting magnets. *International Journal of Heat and Mass Transfer*, 13:105-115.
- [6] Ma Y, Huang C and Wang X (2021) Experimental investigation on boiling heat transfer enhanced by gradient aperture porous copper. *Applied Thermal Engineering*, 191:116877.
- [7] Zhang K, Bai L, Yao G and Wen D (2023) Influence of pore size distribution on pool boiling heat transfer in porous artery structure. *International Journal of Heat and Mass Transfer*, 209:124116.
- [8] Manetti LL, Ribatski G, de Souza RR and Cardoso EM (2020) Pool boiling heat transfer of HFE-7100 on metal foams. *Experimental Thermal and Fluid Science*, 113:110025.
- [9] Yang C-Y and Liu C-F (2013) Effect of coating layer thickness for boiling heat transfer on micro porous coated surface in confined and unconfined spaces. *Experimental Thermal and Fluid Science*, 47:40-47.
- [10] Može M, Zupančič M and Golobič I (2020) Investigation of the scatter in reported pool boiling CHF measurements including analysis of heat flux and measurement uncertainty evaluation methodology. *Applied Thermal Engineering*, 169:114938.